BCSJ

Document type: Article

Selected Paper

Preparation of Sm, Gd and Fe Oxide Nanoparticle-Polydopamine Multicomponent Nanocomposites

Khoa Anh Ton,[1] Yu-Wei Syu,[1] Jun-Jia Xu,[1] and Toyoko Imae*[1,2]

[1]Department of Chemical Engineering, National Taiwan University of Science and Technology, 43 Section 4, Keeling road, Taipei 10607, Taiwan

[2]Graduate Institute of Applied Science and Technology, National Taiwan University of Science and Technology, 43 Section 4, Keelung Road, Taipei 10607, Taiwan

E-mail: imae@mail.ntust.edu.tw

Received: April 19, 2019; Accepted: May 5, 2019; Web Released: June 1, 2019

Toyoko Imae

Toyoko Imae received her doctor of science degree from Nagoya University. She joined the National Taiwan University of Science and Technology, Taiwan, as an honorary chair professor in April 2009, immediately after retiring from Keio University, Japan. She is also professor emeritus of Nagoya University, Japan, since 2006. Her major research areas are the fabrication, functionalization, and physicochemical investigation of nanomaterials, including polymers, nanoparticles, carbon materials, minerals and their composites. Her resent research target is a "Nanoarchitecture and Nanotechnology" towards energy, environmental and biomedical sciences.

Abstract

Nanoparticles of samarium(III) oxide (Sm_2O_3), gadolinium(III) oxide (Gd_2O_3) and iron(II,III) oxide (Fe_3O_4), which have different roles in biomedical applications, were synthesized and embedded in biocompatible polydopamine to make them more dispersible, compatible and non-aggregate so as to fully exploit their features in the human body. Herein, the synthesis procedures of the nanoparticles with different sizes and the embedding procedures in polydopamine were investigated in comparison with coating with silica. The particles (60–100 nm diameter) of Sm_2O_3 and Gd_2O_3 synthesized by the calcination method were coated by silica shell (80–100 nm thickness) but their dispersibility in water was less. The nanosized particles (4–7 nm) of Sm_2O_3 and Gd_2O_3 synthesized by the polyol solvent method were protected by polyol to be dispersed in water. Separately, Fe_3O_4 nanoparticles (17 nm) were fabricated by co-precipitation reaction. Each nanoparticle was successfully embedded into spheres of polydopamine, although the preparation of composites depended on solvent amount, metal precursor amount and reaction solution pH. The co-embedding of three particles in a polydopamine sphere was also proved by elemental analysis.

Keywords: Samarium(III) oxide | Gadolinium(III) oxide | Polydopamine

1. Introduction

For many decades, since cancer is an obsession for humanity, scientists have been continuously discovering new innovations for cancer treatment. A combination of therapeutics and diagnostics, called "theranostics", is one intention. Among current cancer therapies, radiation with a samarium-153 (^{153}Sm) radionuclide is approved to effectively relieve the pain resulting from cancers.[1] ^{153}Sm has a short half-life (1.93 days), it emits therapeutic beta and diagnostic gamma radiation, and its microparticles have a high capacity of labeling and no impurities from neutron activation.[2] Meanwhile, magnetic resonance imaging (MRI) is crucial in order to assess the therapeutic efficacy and identify the tumor characteristics or control the biodistribution of nanocomposites.[3] The development of MRI contrast agents has attracted great attention to gadolinium because of its large number of unpaired electrons and relatively long electronic relaxation.[4] Among the current contrast agents, gadolinium(III) ion is considered as a positive contrast agent and iron oxide as a negative one: They have been encapsulated separately in biodegradable polymer[4,5] or simultaneously in combination as a synergic model to improve the T_1 and T_2 relaxation times.[6] However, instead of using trivalent Gd^{3+} or its derivatives, inorganic nanoparticles are more favorable for preventing renal insufficiency as well as un-inhibiting the calcium channels.

Inspired by the theranostics concept, the integration of different functional nanoparticles into a single biocarrier to overcome the drawbacks of traditional therapy is receiving significant attention. Herein, we focused multifunctional composite structures that simultaneously comprise therapeutic, diagnostic and magnetic imaging agents such as samarium(III) oxide (Sm_2O_3), gadolinium(III) oxide (Gd_2O_3) and iron(II,III)

oxide (Fe_3O_4) embedded in polymers like polydopamine or coated by silica. Traditionally, the surface modification of nanoparticle by silica has been conducted in vast research because of its potential properties such as biocompatibility, hydrophilicity and high labeling efficiency.[7] With respect to polydopamine, since its discovery in 2007,[8] this polymer is widely used for deposition onto the surface of either inorganic or organic substrates, such as carbon fiber-modified polydopamine to improve the dispersibility and compatibility,[9] carbon nanotubes-functionalized polydopamine to reinforce mechanical properties of epoxy resins,[10] antibacterial silver nanoparticles loaded with polydopamine spheres,[11] camptothecin-loaded polydopamine nanoparticles for anti-cancer treatment,[12] polydopamine coated manganese oxide nanoparticles for MRI,[3] Al_2O_3/polydopamine/Ag nanoparticles/Cu microspheres as functional fillers of polymer-based composites and catalysts for industrial reactions,[13] Mn^{2+}-coordinated polydopamine@doxorubicin/poly(lactic-co-glycolic acid) nanoparticles for synergistic chemo-photothermal tumor therapy[14] and iron oxide-coated polydopamine for biomedical application.[15] Therefore, the composite materials containing multi-nanoparticles and biocompatible polymer are a multifunctional platform for requirements of on demand medication to improve health of patients.

In the present research, nanoparticles of Sm_2O_3, Gd_2O_3 and Fe_3O_4 were individually synthesized and integrated singly and finally multiply into a matrix as a carrier. We selected polydopamine as a carrier, because it is known as surface-coverable material. The composite materials embedding simultaneously three nanoparticles may provide functionalities of radiotherapy by Sm_2O_3, thermotherapy (hyperthermia) by Fe_3O_4 and MRI imaging by Gd_2O_3. This combination should open the way for theranostics, that is, the integration (coincidental progress) of therapy and diagnosis.

2. Experimental

Reagents. Samarium(III) nitrate hexahydrate ($Sm(NO_3)_3 \cdot 6H_2O$, 99.9%), gadolinium(III) nitrate hexahydrate ($Gd(NO_3)_3 \cdot 6H_2O$, 99.9%), Iron(II) chloride tetrahydrate ($FeCl_2 \cdot 4H_2O$, 99+%), tetraethyl orthosilicate (TEOS, 98%), diethylene glycol (DEG) ($C_4H_{10}O_3$, 99%) and ethylene glycol (EG) ($C_2H_6O_2$, 99%) were purchased from Acros Organics (Belgium). Iron(III) chloride hexahydrate ($FeCl_3 \cdot 6H_2O$, 98+%) was a product from Sigma-Aldrich (USA). Urea ($CO(NH_2)_2$) was obtained from AppliChemPanreac (Germany). Dopamine hydrochloride ($C_8H_{11}NO_2 \cdot HCl$, 99%) was purchased form Alfa Aesar (United Kingdom). Other reagents were commercial grade. All chemicals were used as received without any purification. Milli-Q (deionized and distilled) water was used throughout the experiments.

Synthesis of Materials. The synthesis process of Sm_2O_3 and Gd_2O_3 nanoparticles followed the calcination method of metal hydroxide and the polyol solvent method.[16,17] So as to synthesize Sm_2O_3 nanoparticles by the calcination method, typically, separately-prepared aqueous solutions (5 ml) of $Sm(NO_3)_3 \cdot 6H_2O$ and urea were mixed at different urea contents and refluxed at 80 °C for 2 h without stirring. After cooling, the mixture was centrifuged for 20 min at 6000 rpm and then the precipitates were washed with butanol, water and ethanol, dried at 90 °C and calcined for 2 h at 650 °C. The synthesis of Gd_2O_3 nanoparticles by the calcination method was performed as follows: Aqueous solution (30 ml) of $Gd(NO_3)_3 \cdot 6H_2O$ (0.1354 g) was poured into an aqueous urea solution (1 M, 30 ml) under stirring. The solution was then heated in an autoclave at 90 °C for 2 h. The obtained precipitate was collected by centrifugation and washed with water several times. The white powder was calcined at 850 °C for 4 h.

For the typical synthesis of Sm_2O_3 nanoparticles by the polyol solvent method, a solution of NaOH (0.125 M, 9 ml) in EG or DEG was added to a solution of $Sm(NO_3)_3 \cdot 6H_2O$ (111 mg, 0.25 mmol) in EG or DEG (9 ml), followed by adjusting pH 11.5 and refluxing at 140 °C under stirring. After 1 h, the temperature was increased to 180 °C and the solution was refluxed under stirring for an additional 1 h. Then the solution changed from colorless to dark brown. The reaction solution was cooled to room temperature and centrifuged to collect the supernatant. Gd_2O_3 nanoparticles were also prepared in DEG. A DEG solution of NaOH (0.25 M, 10 ml) was added to $Gd(NO_3)_3 \cdot 6H_2O$ (0.2 M, 10 ml). The following reaction procedures were the same as those for preparation of Sm_2O_3 nanoparticles. To prepare Fe_3O_4 nanoparticles by the co-precipitation method,[18] $FeCl_3 \cdot 6H_2O$ (83.33 mg) and $FeCl_2 \cdot 4H_2O$ (30.65 mg) were dissolved in water (50 ml), followed by adding an excess amount of an aqueous ammonia solution and stirring strongly. Subsequently, it was heated at 80 °C for 1 h. Fe_3O_4 nanoparticles were collected by using a magnet, washed with water and re-dispersed in water (50 ml) by sonication.

The coating of metal nanoparticles by silica was carried out as follows: Generally, metal oxide nanoparticles (4 mg) were dispersed in isopropanol (20 ml) by ultrasonication for 30 min. Then, water (4 ml), aqueous ammonia solution (NH_4OH 30%, 0.5 ml) and TEOS (15 µl or 20 µl) were added to the dispersion of metal oxide nanoparticles and the mixture was stirred at room temperature for 3 h. The reacted mixture was centrifuged to collect white powder, which was then washed with water and dried.

Polydopamine was produced by the polymerization of dopamine hydrochloride in alkaline conditions.[19] Firstly, an adequate amount of dopamine hydrochloride was dispersed in a mixed solvent of water (70 vol %) and ethanol (30 vol %) with stirring for 30 min. Then, an aqueous ammonia solution (35%) was added to adjust the pH to around 10. The color of solution turned black, which is in response to the formation of polydopamine. After 6 h of reaction, the black powder was separated by centrifugation and washed 3 times with water and ethanol. The same way was employed for the preparation of polydopamine-nanoparticle composites, where the dispersion of as-prepared nanoparticles (1 µl of Sm_2O_3, 1 µl of Gd_2O_3 or/and 50 µl of Fe_3O_4) was added to the mixed solvent before adding dopamine hydrochloride. Scheme 1 illustrates the processes of related chemical reactions.

Characterization. Transmission electron microscopic (TEM) images were produced on a JEOL JEM-2000 FX II instrument (Japan) operated at 120 kV with a scanning transmission electron microscope (STEM) and on a high-resolution transmission electron microscope (HRTEM, Philips Tecnai F30 Field Emission Gun Transmission Microscope, FEG-TEM) operated at 300 kV with an electron diffraction analyzer and an

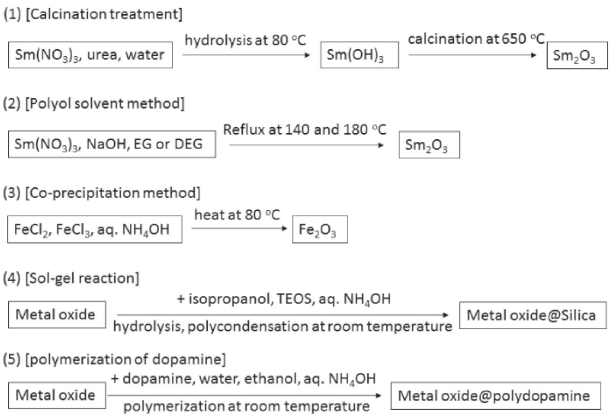

Scheme 1. Illustration of each reaction.

analysis software (Gatan Digital Micrograph (GMS) V1.6.1). A scanning electron microscope (SEM, JSM-6390, Japan) with an energy dispersive X-ray spectrometer (EDS) was operated at an accelerating voltage of 15 kV. X-ray diffraction (XRD) patterns were characterized by a D2 PHASER X-ray diffractometer (BRUKER) and analysis software (EVA V4.1). A dynamic light scattering (DLS, SZ-100, HORIBA Scientific) instrument was operated to obtain the average particle size and the particle size distribution. Infrared absorption (IR) spectra were collected on a Fourier transform infrared absorption spectrometer (Thermo Scientific, Nicolet 6700, USA) at the scanning range of 4000–400 cm^{-1}. A furnace (Thermo Scientific) was used for calcination.

3. Results and Discussion

Synthesis of Sm_2O_3 and Gd_2O_3 by Calcination Treatment and Their Composites with Silica. The hydrolysis of metal ions in the presence of urea as a reaction agent under basic conditions produces metal hydroxide, and the calcination of metal hydroxide yields metal oxide.[20] Through this procedure, spherical nanoparticles of Sm_2O_3 were synthesized, depending on the concentration of urea, which was varied from 0.6 to 1.4 M (see Figure 1A and B): The size decreased from 90.8 ± 7.3–60.9 ± 6.1 nm with increasing urea concentration from 0.6 M to 1.0 M but it was not varied above 1.0 M urea and spherical particles changed to irregular plate-like shape with size larger than 100 nm at 2.0 M urea (data not shown). It may be noticed that the particle size and shape depend on the nuclei formation at the early reaction stage.[21] When the urea concentration increases, the nuclei number increases but the particle size decreases. However, if the nuclei number is too large, the nuclei agglomerates and results in the formation of irregularly shaped particles. Although these particles were prepared under reflux without stirring and the white suspension was resultant, the reacted solution under the reflux with stirring was precipitated and the precipitates were the accumulation of large plates with a few micrometer size (data not shown).

The as-prepared Sm_2O_3 nanoparticles (concentration of urea is 1.0 M and $Sm(NO_3)_3$ is 0.05 M) were not stable in water and they precipitated within one day. Therefore, the Sm_2O_3 nanoparticles were required surface modification to improve the dispersibility in water. A trial was the silica coating of Sm_2O_3 surface, which was performed by the sol-gel reaction with

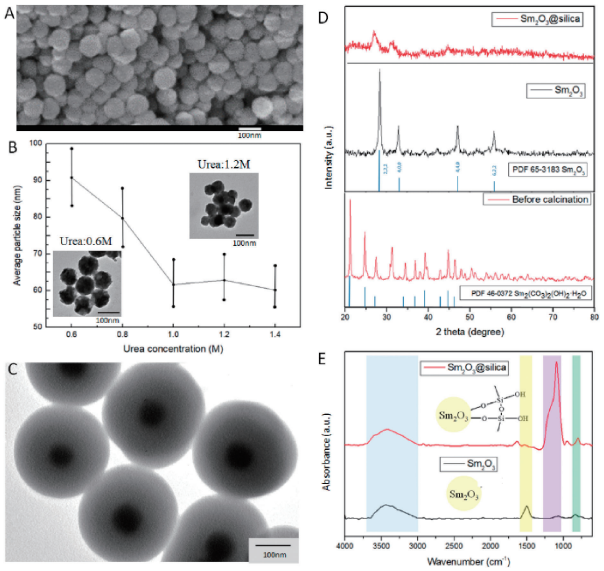

Figure 1. (A) SEM image of Sm_2O_3 prepared by calcination treatment. (B) Variation in average particle size of Sm_2O_3 as a function of urea concentration. Insets are TEM images of Sm_2O_3 at 0.6 and 1.2 M urea. (C) TEM image of Sm_2O_3@silica. (D) XRD patterns of Sm_2O_3 before calcination, Sm_2O_3 and Sm_2O_3@silica with reference patterns. (E) FTIR absorption spectra of Sm_2O_3 and Sm_2O_3@SiO_2.

TEOS. Namely, in the presence of ammonia as a catalyst, TEOS undergoes hydrolysis, following the condensation reaction on the surface of Sm_2O_3 and between hydrolyzed TEOS.[22] A TEM image displayed the composite structure of darker core and lighter shell (Fig, 1C), which were assigned to Sm_2O_3 and silica, respectively, because Sm_2O_3 has significantly high electron density. The core size consisting of Sm_2O_3 was 61.7 ± 6.9 nm, the thickness of silica shell was 103.3 ± 6.6 nm and thus the particle size of composite was 291.5 ± 11.2 nm. The comparison of XRD patterns depending on the synthesized materials is demonstrated in Figure 1D. The XRD pattern displayed that the powder before calcination was a mixture of multiple components including $Sm_2(CO_3)_2(OH)_2H_2O$ (JCPDS card No. 46-0372) but after calcination it changed to Sm_2O_3 cubic crystal (JCPDS card No. 65-3183). However, all the diffraction peaks in the pattern of Sm_2O_3@silica became weak due to the diminution of crystal domains.

The IR absorption spectrum of Sm_2O_3@silica was apparently varied from that of Sm_2O_3 nanospheres (see Figure 1E): The spectrum of Sm_2O_3 showed a broad band at 3443 cm^{-1} and a band at 1502 cm^{-1} attributed to the O-H stretching and bending vibration modes, suggesting the generation of OH group on Sm_2O_3 or the existence of crystallization water in Sm_2O_3.[23] The spectrum of Sm_2O_3 also displayed weak bands at 1093 and 842 cm^{-1} assigned to the stretching vibration modes of Sm–O group.[24] On the other hand, Sm_2O_3@silica revealed a remarkably strong band at 1095 cm^{-1} corresponding to the Si-O-Si stretching vibration mode[25] besides a broad O-H stretching band at 3429 cm^{-1} and a weak Sm–O stretching band at 803 cm^{-1}. Thus, the successful condensation reaction of silanol was supported.

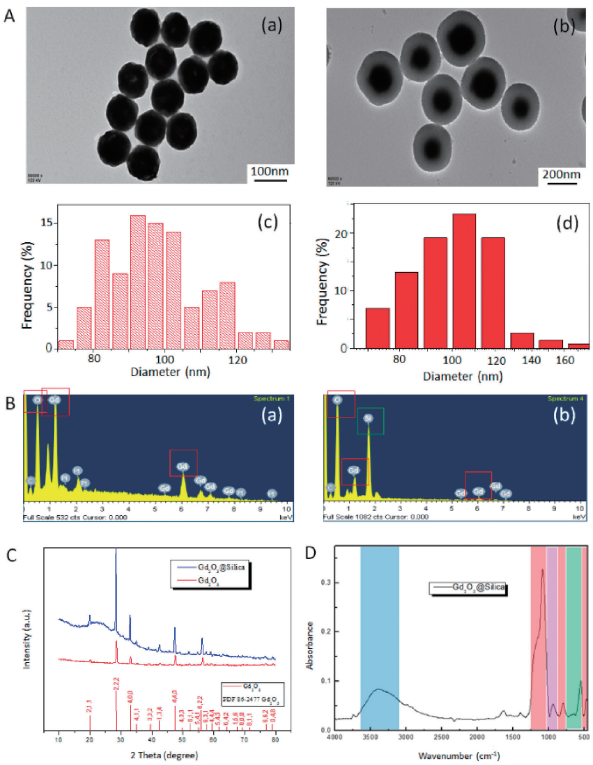

Figure 2. (A) TEM images of (a) Gd_2O_3 and (b) Gd_2O_3@Silica (amount of silica: 15 µl). Particle size distribution of Gd_2O_3 from (c) TEM and (d) DLS. (B) EDS analyses of (a) Gd_2O_3 and (b) Gd_2O_3@Silica. (C) XRD patterns of Gd_2O_3 and Gd_2O_3@silica with reference pattern. (D) An IR absorption spectrum of Gd_2O_3@Silica.

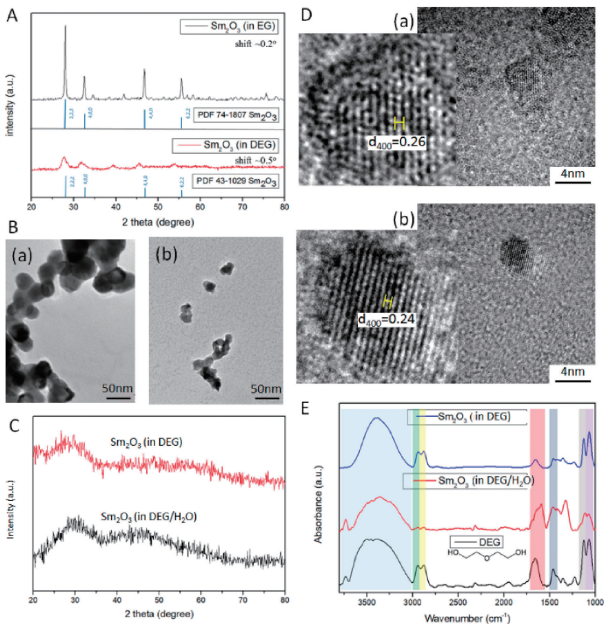

Figure 3. (A) XRD patterns of Sm_2O_3 synthesized by polyol solvent method at 80 °C and calcined at 650 °C with reference patterns. (B) TEM images of Sm_2O_3 synthesized by polyol solvent method at 80 °C in (a) EG and (b) DEG. (C) XRD patterns of Sm_2O_3 synthesized by polyol solvent method at 140/180 °C. (D) HRTEM images of Sm_2O_3 synthesized by polyol solvent method at 140/180 °C in (a) DEG/NaOH and (b) DEG/water. (E) IR absorption spectra of Sm_2O_3 synthesized by polyol solvent method at 140/180 °C in DEG/NaOH and in DEG/water with reference spectrum of DEG.

Under a similar reaction procedure,[20] spherical nanoparticles of Gd_2O_3 were also synthesized (see Figure 2Aa). The histogram of particle size distribution of Gd_2O_3 (Figure 2Ac, d), which was obtained from TEM image and DLS analysis, numerated similar average particle sizes of 95.64 ± 6.83 nm and 101.78 ± 11.31 nm, respectively. Since as-prepared Gd_2O_3 possessed less dispersibility in aqueous medium, an attempt was made to surface-modify the hydrophilic Gd_2O_3 nanoparticles by silica coating.[26] Figure 2Ab shows a TEM image of Gd_2O_3 nanoparticles whose surface was coated with silica shell. Gd_2O_3 core maintained its original size and silica shell homogeneously coated the surface of Gd_2O_3. In addition, when the amount of TEOS was increased from 15 µl to 20 µl at a constant amount of Gd_2O_3 (4 mg), the shell thickness was also increased from 81 to 101 nm. However, the increase in the thickness of silica shell was limited: If excess TEOS was added, single silica spheres were formed without including Gd_2O_3 (data not shown). Incidentally, several conditions such as the reaction time and the amount of ammonia solution or water besides TEOS could control the silica deposition like silica shell thickness.[27]

EDX results in Figure 2Ba,b proved that Gd_2O_3 and Gd_2O_3 with silica shell (Gd_2O_3@Silica) contained elements of gadolinium, oxygen, and silicon. The XRD patterns of Gd_2O_3 and Gd_2O_3@silica are shown in Figure 2C. All the diffraction peaks of both powders can be indexed as the face-centered structure of Gd_2O_3 (JCPDS card no. 86-2477). However, different from Gd_2O_3, Gd_2O_3@silica displayed one additional broad Bragg peak near $2\theta = 25°$, being attributed to SiO_2.[28] These results indicate that the Gd_2O_3 core with single crystallinity is surrounded by the amorphous silica shell and the crystallinity of Gd_2O_3 is not disturbed by the coating of silica shell, different from the case of Sm_2O_3@silica. In the IR spectrum of Gd_2O_3@silica (Figure 2D), an IR absorption band of Gd-O was observed at 544 cm^{-1}, and an absorption band at 942 cm^{-1} corresponds to Si-OH. Three bands at 1090, 797 and 468 cm^{-1} are attributed to Si-O-Si,[29] and a band at 3398 cm^{-1} can be assigned to the OH group of silica shell. These results indicate the successful coexistence of Gd_2O_3 and silica.

The hydrophilicity requirement of Sm_2O_3 and Gd_2O_3 nanoparticles was not completely achieved by means of the silica coating because of the larger size of metal oxide particles. Thus, the improvement is required for particle size.

Synthesis of Sm_2O_3 and Gd_2O_3 by Polyol Solvent Method. Sm_2O_3 nanoparticles were synthesized by polyol solvent method. In the first method, the reaction was performed in two polyols (EG and DEG) at reaction temperature of 80 °C[30] but the XRD pattern showed no Bragg peaks (data not shown) and thus the powder had to be calcined to obtain Sm_2O_3. Then the crystal patterns appeared, as seen in Figure 3A, as compared to JCPDS card no. 74-1807 (cubic structure of Sm_2O_3), although all Bragg peaks of Sm_2O_3 synthesized in DEG were relatively broad as compared to peaks of Sm_2O_3 synthesized in EG. The TEM images (Figure 3B) of Sm_2O_3 from both solvents

showed spherical Sm_2O_3 nanoparticles but the sizes were different between solvents. The size histograms from around 50 randomly selected nanoparticles revealed the mean particle size of 45.3 ± 10.9 nm for EG solvent and 19.5 ± 3.5 nm for DEG solvent. Thus, the higher broadening of XRD peaks of Sm_2O_3 synthesized in DEG comes from its smaller size.

Different from the formation of metal hydroxide at low reaction temperature, the mechanism of the reaction in polyols at high temperature supports the direct production of metal oxide nanoparticles without calcination.[31] Especially, metal nitrate precursor should be preferable to synthesize nanoparticles of quantum size.[32] Moreover, the sizes of nanoparticles and their agglomerates can be changeable by adjusting parameters such as precursor concentration, pH, reaction time, temperature, and additional water.[33] There is a report that the low NaOH concentration is desirable at the start, since NaOH is a preferred donor of hydroxyl ions and the low NaOH concentration results in low reaction yields of hydroxides.[34] In another report, water instead of NaOH has been added to the precursor solution, since DEG is oxidized and loses partly its stabilizing functionality because of the strong oxidizing properties of nitrate ions at high temperature.[35] In fact, when less water was added to a reaction solution, the precipitate was generated but with increasing the amount of water, precipitates decreased. Thus, the second polyol solvent method was carried out in DEG at high temperature by adding low concentration of NaOH (DEG/NaOH) or water (at DEG/water (v/v) ratios of 5).

Figure 3C displays XRD patterns of Sm_2O_3 nanoparticles prepared in DEG/NaOH and DEG/water. The broad peak at around 30° appeared for both nanoparticles correspond to (2,2,2) of Sm_2O_3 crystal. Moreover, another broad peak around 45° corresponding to (4,4,0) appeared in an XRD pattern of Sm_2O_3 nanoparticles prepared in DEG/water. These results indicate that their crystallinity of Sm_2O_3 is poor or its domain is too small. According to HRTEM (Figure 3D), particle sizes were very small to be ~4 nm, but the distinct crystal lattice patterns with the inter atom distance, corresponding to (4,0,0) plane of Sm_2O_3 crystal, appeared at 0.26 nm (d_{400} value is 2.6 Å) for Sm_2O_3 in DEG/NaOH and at 0.24 nm (d_{400} value is 2.4 Å) for Sm_2O_3 in DEG/water. Thus, the broad pattern of XRD originates in the small domain of Sm_2O_3 crystal.

Figure 3E displays a comparison of the IR adsorption spectra of Sm_2O_3 powders synthesized in DEG/NaOH and DEG/water. The IR bands of DEG at 3453, 1663 and 1467 cm^{-1} correspond to the O-H stretching and bending vibration modes of hydroxyl groups and free water. Moreover, DEG showed CH_2 vibration bands at 2943 and 2873 cm^{-1} and the C-O-C skeleton vibration band of alkoxy group and the CO vibration band of hydroxyl group at 1128 and 1067 cm^{-1}.[36] In the case of Sm_2O_3 nanoparticle synthesized in DEG/NaOH, the IR absorption spectrum was completely similar to that of DEG. In the IR absorption spectrum of Sm_2O_3 nanoparticles synthesized in DEG/water, although O-H vibration bands were slightly shifted to lower wavenumbers (3367 and 1598 cm^{-1}), the spectrum was similar to that of DEG. These results indicate that DEG molecules adsorb on Sm_2O_3 nanoparticles. The adsorbed DEG is expected to act as a surface capping agent,[37] which protects Sm_2O_3 nanoparticles to disperse stably in aqueous medium. Similar protection by EG occurred even on ZnO nanoparticles, which was synthesized by the polyol solvent procedure.[17]

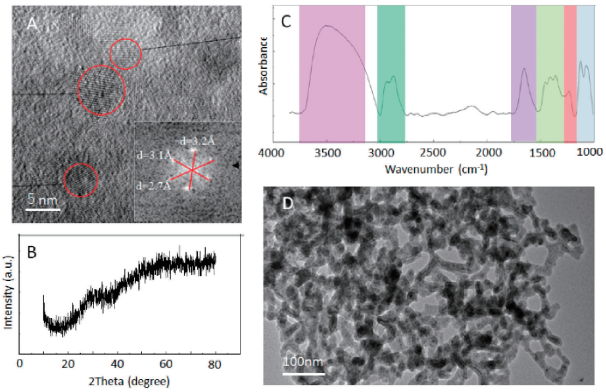

Figure 4. (A) An HRTEM, (B) an XRD pattern and (C) an IR absorption spectrum of Gd_2O_3 prepared by polyol solvent method at 140/180 °C in DEG. (D) A TEM image of Gd_2O_3@silica. Inset in (A) is a Fourier transform of the crystal pattern.

The polyol solvent method was applied even for the synthesis of Gd_2O_3 nanoparticles, since this procedure should produce smaller size of Gd_2O_3 nanoparticles than the calcination method,[37,38] the surface of Gd_2O_3 nanoparticles was coated with DEG and the agglomeration of Gd_2O_3 nanoparticles might be prevented.[39] Gd_2O_3 nanoparticles were synthesized through the same reaction process as Sm_2O_3 nanoparticles,[31] and the particle size of the as-prepared Gd_2O_3 nanoparticles were determined by using HRTEM as shown in Figure 4A. The measured diameter of Gd_2O_3 particles was about 5 nm, which is similar to values previously reported using the same method.[37,38] The particle size of Gd_2O_3 by using the polyol solvent method was much smaller than that from the calcination method described above, as expected. Moreover, the HRTEM image proved the crystalline phase of Gd_2O_3 nanoparticles, and the precise distance of planes was obtained from Fourier transform of the crystal pattern. The different Gd_2O_3 nanoparticles showed the different distances between planes (D values) of 3.2, 3.1 and 2.7 Å. The D values at 3.1 Å and 3.2 Å correspond to the Miller index (2,2,2), and the value at 2.7 Å corresponds to index (4,0,0).[37] The histogram of particle size distribution of Gd_2O_3 by DLS showed the average size of 6.3 ± 0.7 nm.

The XRD pattern of Gd_2O_3 nanoparticles (Figure 4B) showed one weak and broad peak at $2\theta = 29°$ to be an index (2,2,2), corresponding to the small size of Gd_2O_3 nanoparticles. The IR spectrum of Gd_2O_3 nanoparticle is shown in Figure 4C and compared with a spectrum of DEG. Similar IR bands to those of DEG were observed even on a spectrum of Gd_2O_3 prepared in DEG, because DEG was adsorbed on Gd_2O_3. This situation is the same as for Sm_2O_3, as discussed above. The difference of Gd_2O_3 from solvent DEG is the apperance of bands at 1600 and 1550 cm^{-1} because of the contribution of OH groups generated on the surface of Gd_2O_3 nanoparticles.

Moreover, the as-prepared Gd_2O_3 nanoparticles were further surface-modified by using TEOS.[33] A TEM image of Gd_2O_3@silica is shown in Figure 4D. The network of string-like Gd_2O_3@silica was found and it included small particles with

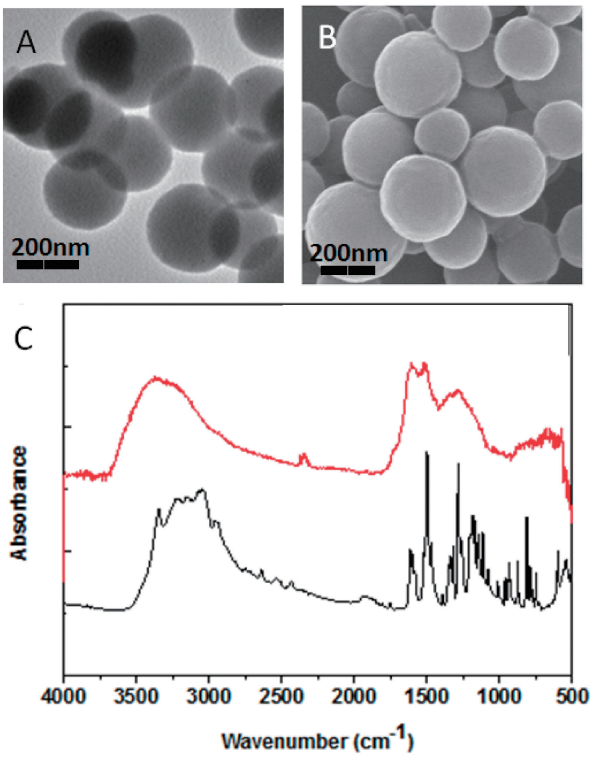

Figure 5. (A) TEM and (B) SEM images of polydopamine. (C) IR absorption spectra of (black) dopamine hydrochloride and (red) polydopamine.

size of around 5 nm, which can be assigned to Gd_2O_3. This indicates the stronger interaction of silanol with OH groups on Gd_2O_3 than the interaction between silanol. Finally, the structure of Gd_2O_3@silica is completely different from that of the composite prepared from the calcination procedure (Figure 2Ab).

Composites of Sm_2O_3, Gd_2O_3 and Fe_3O_4 with Polydopamine. As seen in Fig, 4D, since Gd_2O_3 nanoparticles could not be encapsulated in the spherical silica particles, and alternative biocompatible polymer nanosphere should be considered. Polydopamine was synthesized in the mixed solvent of water and ethanol and its TEM and SEM images are shown in the Figure 5A and B. As expected, the TEM image revealed the spherical shape of polydopamine with average size of 244.3 ± 94.3 nm and the SEM image proved the smooth surface of the spheres. Moreover, polydopamine spheres were well-dispersed in the mixed solvent. Thus, the versatile method with conventional solvents under mild condition is an essential approach for biomedicine.

The IR spectrum of polydopamine is completely different from that of dopamine monomer (Figure 5C). A broad IR absorption band at 3374 cm^{-1} in the IR spectrum of polydopamine is ascribed to the stretching vibration modes of O–H and N–H.[12,13,40] Two bands at 1608 and 1522 cm^{-1} are attributed to C=C stretching and N–H vibration modes of polydopamine, respectively.[11–13,40] The presence of these bands implies that the synthesized polydopamine consists of indole and indoline derivatives produced from the intramolecular cyclization reaction of dopamine.[12,40]

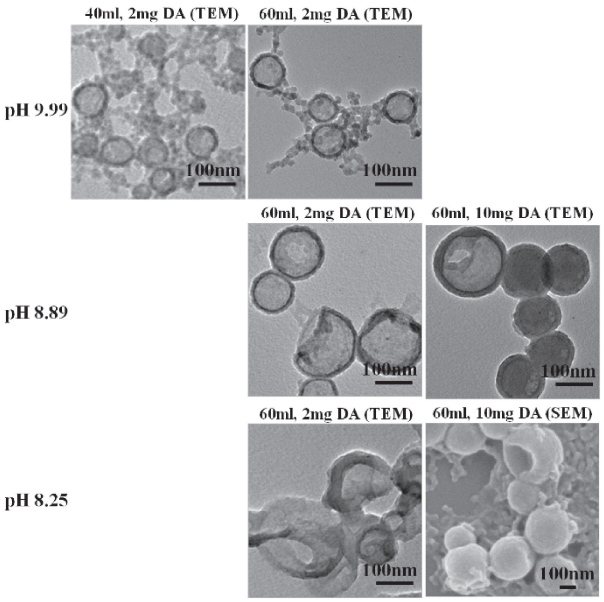

Figure 6. TEM images of Sm_2O_3@polydopamine at different volumes of solvent (40 and 60 ml), pH (9.99, 8.89 and 8.25) and amount of dopamine hydrochloride (2 and 10 mg). A SEM image of Sm_2O_3@polydopamine at 60 ml of solvent volume, pH 8.89 and 10 mg of dopamine hydrochloride.

Since the formation of spherical polydopamine particles was confirmed, subsequently, nanoparticles of Sm_2O_3, Gd_2O_3 and Fe_3O_4 were embedded in polydopamine. Nanoparticles of Sm_2O_3 and Gd_2O_3 were synthesized by means of the polyol solvent method and the nanoparticle of Fe_3O_4 was synthesized by the co-precipitation method. The average sizes of Sm_2O_3, Gd_2O_3 and Fe_3O_4 determined from DLS analysis were 7.0 ± 0.5, 4.4 ± 0.5, and 16.8 ± 4.2 nm, respectively.

TEM images of Sm_2O_3@polydopamine composites are shown in Figure 6. The morphology of composites depended on the volume of solvent, the amount of dopamine and a pH of the reaction solution. The composites prepared with 2 mg of dopamine at pH 9.99 considerably varied in size and shape, depending on the volume of solvent from 20 to 100 ml, that is, following the increase of water content. At solvent volume of 20 and 30 ml, polydopamine embedded Sm_2O_3 nanoparticles, and the nanoparticle-embedded polydopamine seemed to be inter-connected (no data shown). When the volume of solvent was increased to 40–60 ml, the bigger spheres appeared along with interconnected Sm_2O_3-embedded polydopamine. However, the interconnection among bigger spheres increased at higher volumes of solvent than 60 ml (no data shown).

Figure 6 also illustrates the change in size of Sm_2O_3@polydopamine composites at 60 ml of solvent volume and 2 mg of dopamine depending on pH. The decrease of pH from 9.99 to 8.89 and 8.25 resulted in the increase of size of spherical composites. At the same time, different from the case of high pH (at 9.99), the particle shape was distorted from that of a real sphere at pH 8.25, and the production of the interconnected Sm_2O_3-embedded polydopamine dramatically decreased at pH 8.89 and 8.25. It has been reported that the size of polydopamine is controllable by altering the pH of the reaction

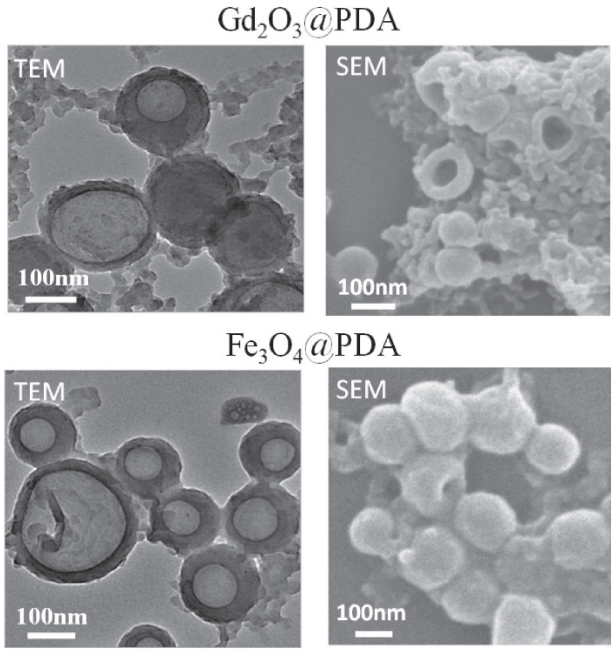

Figure 7. TEM and SEM images of Gd_2O_3@polydopamine (60 ml solvent, pH 8.89, 10 mg dopamine) and Fe_3O_4@polydopamine (60 ml solvent, pH 8.89, 12 mg dopamine).

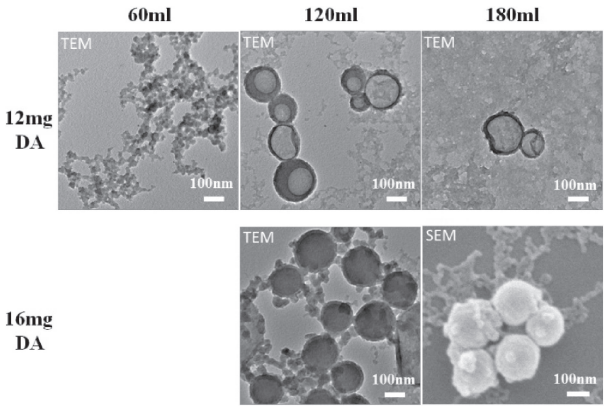

Figure 8. TEM images of $Sm_2O_3/Gd_2O_3/Fe_3O_4$@polydopamine at pH 8.89 with volume (60, 120 and 180 ml) of solvent and amount (12 and 16 mg) of dopamine hydrochloride. A SEM image of $Sm_2O_3/Gd_2O_3/Fe_3O_4$@polydopamine at pH 8.89 with 120 ml solvent and 16 mg dopamine hydrochloride.

mixture, being without the dramatic effect on the morphology.[11,12,41] Moreover, Ho and Ding[12] explained the size change by the kinetic constant of self-polymerization depending on pH: The reaction kinetic constant is low at lower pH in comparison with at higher pH, and this is less advantageous for accelerating the nucleation of polydopamine particles, and the reaction produces polydopamine spheres in large diameter with high yield.

Compared to spherical particles at 2 mg dopamine at pH 8.89, the increase of dopamine to 10 mg made the spheres not only bigger in diameter but also rigid and dense. From the SEM image of the same Sm_2O_3@polydopamine, the texture of the broken hollow particles was observed with major spherical particles (see Figure 6). Therefore, it is now clear that the size of Sm_2O_3@polydopamine composite nanoparticles can be controlled by the concentration of dopamine, besides the volume of solvent and the pH of solution,[42] and the shape and rigidity of composite nanoparticles also controlled by modifying these factors.

For Gd_2O_3@polydopamine composites at 60 ml solvent volume and pH 8.89, there was obvious evidence for the effect of increasing the dopamine amount from 2 to 6 and 10 mg, that is, for changes in size and shape of composite nanoparticles: The interconnected Gd_2O_3-coated polydopamine and the hollow sphere were the majority at 2 and 6 mg, respectively (no data shown) and composites at 10 mg were the coexistence of hollow sphere, hard sphere and minor interconnected Gd_2O_3-embedded polydopamine (Figure 7). The SEM image agrees with the result from TEM.

A similar dopamine concentration dependency was also obtained for composites of Fe_3O_4@polydopamine. At a small amount (6 mg) of dopamine, Fe_3O_4 nanoparticles were embedded in the polydopamine matrix but the shape the matrix was not clearly spherical (no data shown). Hollow spheres were formed at the existence of 12 mg dopamine and this shape was not varied even at 18 mg, as being obvious in TEM and SEM images of Figure 7.

For synergetic theranostic applications, the co-embedding of three metal nanoparticles into polydopamine is highly anticipated. Figure 8 shows TEM images at 12 mg dopamine, pH 8.89 and various volumes of solvent. The nanoparticle-embedded polydopamine agglomerated at low volume of solvent (60 ml). When the volume of solvent was increased to 120 ml, hollow spheres were formed but the further increase of the volume to 180 ml decreased the number of hollow spheres. Thus, the volume of solvent strongly effects on the morphology of three metal nanoparticle composites.

Besides, as mentioned above, the amount of dopamine also can control the formation of composite particles. Consequently, when the TEM image and the size distribution of composite at 120 ml solvent and pH 8.89 were compared between dopamine amounts of 12 mg and 16 mg, the hard spheres were visualized for composites at 16 mg dopamine (Figure 8). SEM images (Figure 8) also supported the formation of hard spheres. This tendency to form hard spheres was similar to the dopamine amount dependency on single metal nanoparticle@polydopamine composites as described above. It should be noticed that the $Sm_2O_3/Gd_2O_3/Fe_3O_4$@polydopamine composites in this optimum condition were well dispersed in water. This is to be expected because polydopamine has hydrophilic functional groups such as hydroxyl and amine groups.[43]

The aforementioned experimental results allowed elucidation of the conditions to obtain hard sphere composite particles of $Sm_2O_3/Gd_2O_3/Fe_3O_4$@polydopamine. To prove the co-embedding of three nanoparticles in a polydopamine sphere, XRD of polydopamine, Sm_2O_3@polydopamine, Gd_2O_3@polydopamine, Fe_3O_4@polydopamine and $Sm_2O_3/Gd_2O_3/Fe_3O_4$@polydopamine was measured. As seen in Figure 9, a broad Bragg peak at 23.3° of polydopamine was observed but no Bragg peaks from metal oxide nanoparticles were detected even after embedding nanoparticles, because the amounts of

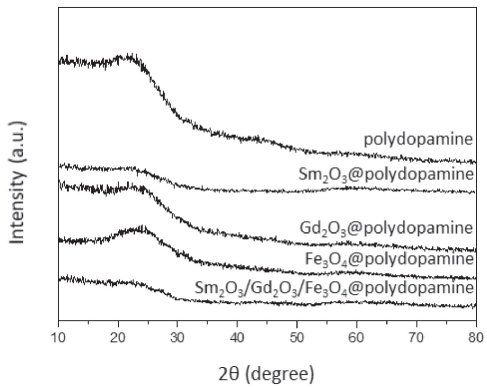

Figure 9. XRD patterns of polydopamine, Sm_2O_3@polydopamine, Gd_2O_3@polydopamine, Fe_3O_4@polydopamine and $Sm_2O_3/Gd_2O_3/Fe_3O_4$@polydopamine.

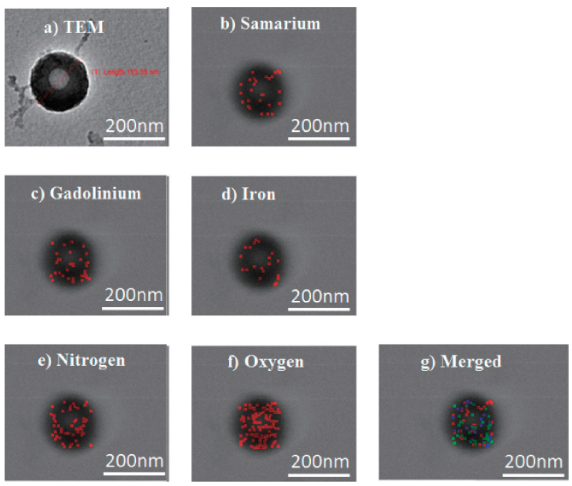

Figure 10. STEM images and EDS location maps of $Sm_2O_3/Gd_2O_3/Fe_3O_4$@polydopamine (12 mg dopamine, 120 ml solvent and pH 8.89). Colors in merged figure (g) are red for Sm_2O_3, green Gd_2O_3 and blue for Fe_3O_4.

metal oxides were less than 1 wt % of polydopamine. Thus, the determination of the co-embedding of three nanoparticles in a polydopamine sphere was not achieved using XRD.

Thus, so as to evaluate the colocalization of metal oxide nanoparticles in the sphere, EDS mapping was performed. In the STEM image of polydopamine sphere in Figure 10a, five elements of Sm, Gd, Fe, C and O were mapped as shown in Figure 10b–f and merged in Figure 10g. The maps showed five elements that are present in the interior of a single sphere. Herein, oxygen belongs to metal nanoparticles and polydopamine, and nitrogen is in polydopamine. Thus, it was confirmed that three kinds of nanoparticles (Sm_2O_3, Gd_2O_3 and Fe_3O_4) were co-distributed in the internal domain of the nanocomposite sphere.

The coexistence of Fe_3O_4 nanoparticles in polydopamine can be proved by means of a magnet. Figure 11 shows the phenomenon of Fe_3O_4@polydopamine and $Sm_2O_3/Gd_2O_3/Fe_3O_4$@polydopamine dispersions under the absence and presence of magnet. The composites in Fe_3O_4@polydopamine dispersion were attracted by the magnet, and the same phenomenon was observed even for $Sm_2O_3/Gd_2O_3/Fe_3O_4$@polydopamine dispersions, indicating their magnetic properties because of the existence of Fe_3O_4 nanoparticles in both dispersions.

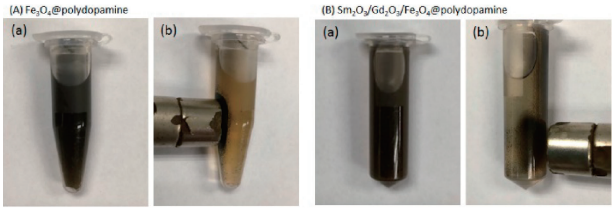

Figure 11. The behaviors of composites in (A) Fe_3O_4@polydopamine and (B) $Sm_2O_3/Gd_2O_3/Fe_3O_4$@polydopamine dispersions under the (a) absence and (b) presence of magnet.

4. Conclusion

A feasible method to create a composite nanosphere as multifunctional nanomaterial for clinical utilization in theranostics was developed. The therapeutic Sm_2O_3 and diagnostic Gd_2O_3 nanoparticles were synthesized by the calcination procedure producing 60–70 nm spherical particles, which were then coated with silica but they showed poor dispersibility in water. On the other hand, particles prepared by the polyol solvent method were in the nanoscale of range 4–7 nm. They were embedded simultaneously with Fe_3O_4 in polydopamine nanosphere. Elemental analysis indicated that the nanoparticles were distributed in the domain of polydopamine. This composite material took the spherical shape and well-dispersed in water. These results indicate the ability of polydopamine as a biodegradable carrier of nanoparticles for synergic theranostics.

KAT gratefully acknowledges financial support from National Taiwan University of Science and Technology, Taiwan, in the form of a student scholarship.

References

1 Y. Parlak, G. Gumuser, E. Sayit, in *Prostate Cancer—Leading-edge Diagnostic Procedures and Treatments*, ed. by R. Mohan, InTech, Rijeka, **2016**, Ch. 07. doi:10.5772/64670.

2 N. A. A. Hashikin, C.-H. Yeong, B. J. J. Abdullah, K.-H. Ng, L.-Y. Chung, R. Dahalan, A. C. Perkins, *PLoS One* **2015**, *10*, e0138106.

3 X. Ding, J. Liu, J. Li, F. Wang, Y. Wang, S. Song, H. Zhang, *Chem. Sci.* **2016**, *7*, 6695.

4 Y.-S. Lin, Y. Hung, J.-K. Su, R. Lee, C. Chang, M.-L. Lin, C.-Y. Mou, *J. Phys. Chem. B* **2004**, *108*, 15608.

5 Z. Chen, D. Yu, C. Liu, X. Yang, N. Zhang, C. Ma, J. Song, Z. Lu, *J. Drug Targeting* **2011**, *19*, 657.

6 R. Di Corato, F. Gazeau, C. Le Visage, D. Fayol, P. Levitz, F. Lux, D. Letourneur, N. Luciani, O. Tillement, C. Wilhelm, *ACS Nano* **2013**, *7*, 7500.

7 T. Kim, E. Momin, J. Choi, K. Yuan, H. Zaidi, J. Kim, M. Park, N. Lee, M. T. McMahon, A. Quinones-Hinojosa, J. W. M. Bulte, T. Hyeon, A. A. Gilad, *J. Am. Chem. Soc.* **2011**, *133*, 2955.

8 J. H. Ryu, P. B. Messersmith, H. Lee, *ACS Appl. Mater. Interfaces* **2018**, *10*, 7523.

9 S. Chen, Y. Cao, J. Feng, *ACS Appl. Mater. Interfaces* **2014**, *6*, 349.

10 Y. Ling, W. Li, B. Wang, W. Gan, C. Zhu, M. A. Brady, C. Wang, *RSC Adv.* **2016**, *6*, 31037.

11 H. Luo, C. Gu, W. Zheng, F. Dai, X. Wang, Z. Zheng, *RSC Adv.* **2015**, *5*, 13470.
12 C.-C. Ho, S.-J. Ding, *J. Mater. Sci.: Mater. Med.* **2013**, *24*, 2381.
13 J. Hu, S. Wu, Q. Cao, W. Zhang, *RSC Adv.* **2016**, *6*, 81767.
14 J. Xi, L. Da, C. Yang, R. Chen, L. Gao, L. Fan, J. Han, *Int. J. Nanomed.* **2017**, *12*, 3331.
15 D. Liu, L. Ma, L. Liu, L. Wang, Y. Liu, Q. Jia, Q. Guo, G. Zhang, J. Zhou, *ACS Appl. Mater. Interfaces* **2016**, *8*, 24455.
16 B. Krishnakumar, T. Imae, *Appl. Catal., A* **2014**, *486*, 170.
17 M. T. Efa, T. Imae, *J. Taiwan Inst. Chem. Eng.* **2018**, *92*, 112.
18 M. C. Mascolo, Y. Pei, T. A. Ring, *Materials* **2013**, *6*, 5549.
19 X. Jiang, Y. Wang, M. Li, *Sci. Rep.* **2014**, *4*, 6070.
20 E. Matijević, W. P. Hsu, *J. Colloid Interface Sci.* **1987**, *118*, 506.
21 M.-Y. Cheng, D.-H. Hwang, H.-S. Sheu, B.-J. Hwang, *J. Power Sources* **2008**, *175*, 137.
22 Y. Kobayashi, H. Katakami, E. Mine, D. Nagao, M. Konno, L. M. Liz-Marzán, *J. Colloid Interface Sci.* **2005**, *283*, 392.
23 Y. Ikeda, T. Imae, J. Hao, M. Iida, T. Kitano, N. Hisamatsu, *Langmuir* **2000**, *16*, 7618.
24 J. Gao, Y. Zhao, W. Yang, J. Tian, F. Guan, Y. Ma, J. Hou, J. Kang, Y. Wang, *Mater. Chem. Phys.* **2003**, *77*, 65.
25 A. Shishmakov, O. V. Koryakova, A. S. Seleznev, L. A. Petrov, S. A. Melkozerov, *Russ. J. Appl. Chem.* **2013**, *86*, 151.
26 A. Jain, G. A. Hirata, M. H. Farías, F. F. Castillón, *Nanotechnology* **2016**, *27*, 065601.
27 S. Santra, R. Tapec, N. Theodoropoulou, J. Dobson, A. Hebard, W. Tan, *Langmuir* **2001**, *17*, 2900.
28 B. Liu, D.-P. Wang, W.-H. Huang, A.-H. Yao, I. Koji, *J. Inorg. Mater.* **2008**, *23*, 33.
29 M. T. Kim, *Thin Solid Films* **1997**, *311*, 157.
30 S. S. Alias, A. B. Ismail, A. A. Mohamad, *J. Alloys Compd.* **2010**, *499*, 231.
31 J. Yang, C. Li, Z. Quan, D. Kong, X. Zhang, P. Yang, J. Lin, *Cryst. Growth Des.* **2008**, *8*, 695.
32 B. Mutelet, P. Perriat, G. Ledoux, D. Amans, F. Lux, O. Tillement, C. Billotey, M. Janier, C. Villiers, R. Bazzi, S. Roux, G. Lu, Q. Gong, M. Martini, *J. Appl. Phys.* **2011**, *110*, 094317.
33 M. A. Flores-Gonzalez, G. Ledoux, S. Roux, K. Lebbou, P. Perriat, O. Tillement, *J. Solid State Chem.* **2005**, *178*, 989.
34 R. Bazzi, A. Brenier, P. Perriat, O. Tillement, *J. Lumin.* **2005**, *113*, 161.
35 K. Lebbou, P. Perriat, O. Tillement, *J. Nanosci. Nanotechnol.* **2005**, *5*, 1448.
36 G. Azizian, N. Riyahi-Alam, S. Haghgoo, H. R. Moghimi, R. Zohdiaghdam, B. Rafiei, E. Gorji, *Nanoscale Res. Lett.* **2012**, *7*, 549.
37 R. Bazzi, M. A. Flores, C. Louis, K. Lebbou, W. Zhang, C. Dujardin, S. Roux, B. Mercier, G. Ledoux, E. Bernstein, P. Perriat, O. Tillement, *J. Colloid Interface Sci.* **2004**, *273*, 191.
38 R. M. Petoral, F. Söderlind, A. Klasson, A. Suska, M. A. Fortin, N. Abrikossova, L. Selegård, P.-O. Käll, M. Engström, K. Uvdal, *J. Phys. Chem. C* **2009**, *113*, 6913.
39 S. Riyahi-Alam, S. Haghgoo, E. Gorji, N. Riyahi-Alam, *Iran. J. Pharm. Res.* **2015**, *14*, 3.
40 N. Nishizawa, A. Kawamura, M. Kohri, Y. Nakamura, S. Fujii, *Polymers* **2016**, *8*, 62.
41 K.-Y. Ju, Y. Lee, S. Lee, S. B. Park, J.-K. Lee, *Biomacromolecules* **2011**, *12*, 625.
42 J. Yan, L. Yang, M.-F. Lin, J. Ma, X. Lu, P. S. Lee, *Small* **2013**, *9*, 596.
43 C. Shi, C. Deng, X. Zhang, P. Yang, *ACS Appl. Mater. Interfaces* **2013**, *5*, 7770.